Nereis. Revista Iberoamericana Interdisciplinar de Métodos, Modelización y Simulación	9	25-38	Universidad Católica de Valencia San Vicente Mártir	Valencia (España)	ISSN 1888-8550

Calculation of Restricted Volume for Nanoparticles that Can Point

Cálculo del volumen restringido para nanopartículas que pueden orientarse

Fecha de recepción y aceptación: 15 de enero de 2017 y 25 de febrero de 2017.

Francisco Torrens Zaragozá[1*]

[1] Institut Universitari de Ciència Molecular. Universitat de València.
* Correspondencia: Edifici d'Instituts de Paterna, P. O. Box 22085. 46071 València. España. *E-mail:* torrens@uv.es.

ABSTRACT

Nanoparticles' restricted volume affects the phase behaviour of polymer/disc nanocomposites. The so-called b-parameter is defined as half of the excluded volume between particles and is equal to half of the volume occupied by one particle when rotating in all directions. This report presents the calculation of b-parameter for particles of different geometric shapes: a rod, a disc (circular sheet), a parallelepipedic sheet, an equilateral-triangular sheet and a regular-hexagonal sheet, extending the calculation of the restricted volume of disc particles to others with different forms, in order to calculate composites phase diagrams. The comparison of nanodiscs with nanoclay indicates that further aggregation models are needed.

KEYWORDS: *Intercalation compound, Polymer nanocomposite, Orientation, Phase diagram, Nanoparticle, Nanosheet, Nanoindentation, Nanodispersion, Organophilic, Montmorillonite, Nanoclay, Nanofil® 919, Layered silicate, Phyllosilicate, Organically modified silicate, Organophilization.*

RESUMEN

El volumen restringido de las nanopartículas afecta al comportamiento de las fases de nanocompuestos polímero/disco. El llamado parámetro-*b* se define como la mitad del volumen excluido entre partículas y es igual a la mitad del volumen ocupado por una partícula cuando gira en todas direcciones. Este informe presenta el cálculo del parámetro *b* para partículas de diferentes formas geométricas: una varilla, un disco (lámina circular), una lámina paralelepipédica, una lámina triangular equilátera y una lámina hexagonal regular, extendiendo el cálculo del volumen restringido de partículas discoidales a otras de diferentes formas para calcular los diagramas de fase de los compuestos. La comparación de nanodiscos con nanoarcilla indica que se necesitan más modelos de agregación.

PALABRAS CLAVE: *Compuesto de intercalación, Nanocompuesto polimérico, Orientación, Diagrama de fase, Nanopartícula, Nanolámina, Nanomella, Nanodispersión, Organofílico, Montmorillonita, Nanoarcilla, Nanofil® 919, Silicato a capas, Filosilicato, Silicato modificado orgánicamente, Organofilización*.

INTRODUCTION

Thermoplastic polymers, *e.g.*, general-purpose (GP) polystyrene (PS, GPPS), are stiff and brittle. They are in a solid (glassy) state at room temperature (RT) but flow if heated above glass transition temperature T_g. They turn back rigid when cooled. Their main advantages are easiness of use and low cost. Their main disadvantages are low resistance to high temperature and modest mechanical strength. Their properties are determined by short-range van der Waals (VdW) attractions between polymers chains. Since molecules are long hydrocarbon (HC) chains (HCCs) that consist of thousands of atoms, total attraction is large. When heated (or rapidly deformed because of a combination of viscoelastic and thermal insulation properties), chains are able to take on a higher degree of conformation and slide past one another.

The *intermolecular* weakness (*vs*. high *intramolecular* strength because of HCC) confers flexibility and elasticity. System ability to be readily deformed above T_g allows thermoplastic polymers to be promptly softened and molded upon heating. Pure thermoplastic polymers are brittle, but hard enough that a fairly high-performance product can be made by giving it some properties of a stretchier material, *e.g.*, rubber, making a co-polymer. In order to improve their mechanical strength, a rubber can be added up to a 14% during polymerization. Epoxy resins produce thermosetting polymers. All thermosetting polymers present a low impact strength and for that reason commonly contain fillers. In order to improve toughness and thermal resistance, the addition of nano-sized filler particles is a common practice, because it improves not only the mechanical properties but also reduces cost.

A small amount of thermoplastic co-polymer poly(styrene-*b*-methyl methacrylate) [P(S-*b*-MMA)], mixed with PS, made mixtures compatible with epoxy resin and polymer [1]. Curing agent was aromatic diamine 4,4'-methylenebis(2,6-diethylaniline) (MDEA). Sheet nanoparticles (NPs, nanosheets) were nanoclay Na-montmorillonite (MMT-Na^+) Nanofil® 757 (N757) and organophilic N919 [modified with $CH_3–(CH_2)_{17}–N^+(CH_3)_2CH_2–C_6H_5Cl^–$]. Filler interacting with polymers contained a single HCC. Nanodispersions were polymer/layer silicate nanocomposites (NCs). Mixture preparation, and test and measurement equipment were described. Balazs model extended to monomer/polymer/clay composites obtained free energy [2]. Minimizing free energy and calculating chemical potentials of the three components, phase diagrams (PDs) for monomer/disc and monomer/polymer/disc mixtures were built. Comparing PDs, effects of nanodisc size, polymer molar mass and interaction parameters were studied on mixture stability and morphology. The PDs were calculated *vs*. polymer length, disc aspect ratio diameter/thickness and polymer molecular mass, for monomer/disc and polymer/disc mixtures at a number of discs compositions. Mixture morphology was discussed and conclusions, obtained from experiments on mixtures of clays and epoxy monomer, or disc and styrene polymer of high molecular mass, were compared, showing qualitative agreement. Equations were generalized to polymer/disc blends to examine the effect of small monomer on miscibility, and apply it to epoxy resin and disc mixtures [3]. The influence of the curing temperature of clay/epoxy NCs on morphology, mechanical properties and free volume was reported [4].

In an earlier publication, negatively co-operative binding of apitoxin (bee venom) peptide melittin to neutral phospholipid vesicles and stability of pairs of colloidal particles [Derjaguin–Landau–Verwey–Overbeek (DLVO) theory] were reported [5]. In *Nereis*, polymer bisphenol-A (BPA), incorporation of silica (SiO_2) nanospheres (nanosilica, nano-SiO_2) into epoxy/amine materials and polymer NCs were informed [6]. The aim of the present report is to review the modelling of the phase behaviour of monomer/disc NCs. The purpose is to present a compatibility with the matrix to improve its mechanical properties. The main objective is to generalize the calculation of the restricted volume of disc NPs to different shapes: rod, and parallelepipedic, equilateral-triangle and regular-hexagonal sheets to calculate NCs PDs.

COMPUTATIONAL METHOD

Background

Polymer is modelled as length-N flexible chains. Monomer diameter a is length unit: $a \cdot x = N$, where x is polymerization degree. As mixture is assumed incompressible, polymer volume fraction $\phi_p = 1 - \phi_d$, where ϕ_d is discs volume fraction [7]. Rotating discs cause two equilibrium miscible regions: they are randomly oriented making isotropic phase (IP, *i*) or lined up forming nematic phase (NeP, *n*). Examining one-polymer/disc miscibility and structural phase configuration [8–10], Onsager model supposes that discs and chains move freely to equilibrate the system, needing a free volume [11]. It describes liquid crystal order and Ginzburg formalism explains polymer/polymer interactions. Mixing free energy is:

$$\Delta G = \Delta G_{conf} + \Delta G_{ster} + \Delta G_{int} + \Delta G_{transl} \quad (1)$$

where ΔG_{conf} describes the conformational losses because of discs alignment:

$$\Delta G_{conf} = n_d \int f(\mathbf{u}) \ln\left[4\pi f(\mathbf{u})\right] d\Omega_u = n_d(\delta + \text{const}) \tag{2}$$

where n_d is the number of discs in a unit volume, and f(u), the orientational distribution function. Onsager used the variational method with a trial function for f(u):

$$f(\mathbf{u}) = \frac{\alpha}{4\pi} \exp\left(-\frac{\alpha\theta^2}{2}\right) \tag{3}$$

where α is a variational parameter, and θ, director/test-disc angle. Parameter δ decides IP/NeP. In IP, δ = 0, while in NeP:

$$\delta_n = 2\ln\left[-\frac{2}{\pi^{1/2}} \frac{b}{v_d} \ln\left(1-\phi_d\right)\right] - 1 \tag{4}$$

where $b = \pi^2 D^3/16$ is half of excluded volume between two randomly oriented discs (*cf.* Subsection Method of Calculation of *b*-Parameter for Nanoparticles that Can Point), $v_d = \pi D^2 L/4$, disc volume, and D and L, disc diameter and length. Term ΔG_{ster} represents discs *steric* interactions [12–14], which represent nonideal entropic free energy:

$$\begin{aligned} \Delta G_{ster} &= n_d J(\phi_d) \iint f(\mathbf{u}_1) f(\mathbf{u}_2) B(\gamma) d\Omega_1 d\Omega_2 \\ &= -\frac{n_d}{v_d} \ln\left(1-\phi_d\right) \iint \frac{\alpha^2}{16\pi^2} \exp^2\left(-\frac{\alpha\theta^2}{2}\right) b \frac{4}{\pi} |\sin\gamma| d\Omega_1 d\Omega_2 = -\frac{n_d}{v_d} \ln\left(1-\phi_d\right) b\rho \end{aligned} \tag{5}$$

where $J(\phi_d) = -(1/v_d)\ln(1-\phi_d)$ extends the model beyond discs low-concentrations limit, $B(\gamma) = b(4/\pi)|\sin\gamma|$, second virial coefficient, γ, discs angle and $\rho = (4/\pi)\langle|\sin\gamma|\rangle$. The $B(\gamma)$ is related to the validity of ideality *vs*. discs concentration; *e.g.*, small $B(\gamma)$ increases discs concentration limit for ideality; if $B(\gamma)$ changes sign *vs*. temperature, a temperature exists at which $B(\gamma)$ is zero, increasing discs concentration limit of ideality. Phase equilibria of a polydisperse hard-disc system were investigated by Monte Carlo [15]. Term ΔG_{int} accounts for nonspecific discs attractions:

$$\Delta G_{int} = -\phi_d b(n_d/v_d)(\Theta/T) \tag{6}$$

Parameter Θ stands for theta temperature and T, absolute one. Temperature Θ is that at which components are not interacting, so system is in stable limit. For $T = \Theta$, $B(\gamma)$ is zero. For polymer/disc mixtures, Θ depends on enthalpic contribution χ and entropic losses for length-N polymers [16]. Term ΔG_{transl} represents discs translational entropy:

$$\Delta G_{transl} = n_d \ln\phi_d \tag{7}$$

From Eqs. (1), (2) and (5)–(7), ΔG, in kT units, where k is the Boltzmann constant, turns out to be:

$$\begin{aligned} \Delta G &= n_d\delta - \frac{n_d}{v_d}\ln\left(1-\phi_d\right) b\rho - \phi_d b \frac{n_d}{v_d}\frac{\Theta}{T} + n_d \ln\phi_d + \text{const} \cdot n_d \\ &= n_d\left[\text{const} + \ln\phi_d + \delta - \ln\left(1-\phi_d\right)\frac{b}{v_d}\rho - \phi_d \frac{b}{v_d}\frac{\Theta}{T}\right] \end{aligned} \tag{8}$$

Determining constant *const*, one expresses Θ/T in terms of Flory-Huggins (FH) interaction parameter χ, equating Eq. (8) in the isotropic case ($\delta = 0$, $\rho = 1$) with the free energy of an isotropic mixture [17]:

$$\Delta G = n_d \ln\phi_d + n_p \ln\phi_p + \chi n_d v_d \phi_p \tag{9}$$

where n_p is number of polymer molecules in a unit volume. Assuming that IP is stable for low discs concentrations and these to expand logarithmic terms, equating Eq. (8) with (9) results:

$$\frac{\Theta}{T} = 1 + \left(\chi - \frac{N}{2}\right)\frac{v_d^2}{b} \tag{10}$$

with $\chi = 1/2$ for $T = \Theta$ if $N = 1$. Equation (10) is obtained if in Eq. (8):

$$\text{const} = \chi v_d - \frac{n_p}{n_d}\phi_d - \frac{N}{2} v_d \phi_d = \chi v_d - \frac{v_d}{v_p}\phi_p - \frac{v_p}{2} v_d \phi_d \tag{11}$$

is reduced to $const \approx \chi v_d$ for low discs concentrations. Substituting Eq. (10) into (8) gives:

$$\Delta G = n_d \left[\text{const} + \ln\phi_d + \delta - \ln\left(1-\phi_d\right)\frac{b}{v_d}\rho - \phi_d \frac{b}{v_d} - \chi v_d \phi_d + v_d \phi_d \frac{N}{2}\right] \tag{12}$$

Substituting Eq. (11) into (12), in view of $-n_p\phi_d \approx n_p \ln\phi_p$ and $N = v_p$ (volume of a polymer molecule), free energy results:

$$\Delta G = n_d \left[\text{const} + \ln\phi_d + \delta - \ln\left(1-\phi_d\right)\frac{b}{v_d}(\rho - 1) + \chi v_d \phi_p\right] + n_p \ln\phi_p \tag{13}$$

Making cloud points in PD, one equates the chemical potentials of system components polymer and discs in IP and NeP:

$$\mu_p^i = \mu_p^n \tag{14}$$

$$\mu_d^i = \mu_d^n \tag{15}$$

where:

$$\mu_p = \left(\frac{\partial \Delta G}{\partial n_p}\right)_{\text{pressure},T,n_d} = -\frac{N}{v_d}\left[\phi_d + \frac{\phi_d^2}{1-\phi_d}\frac{b}{v_d}\rho - \phi_d^2 \frac{b}{v_d}\frac{\Theta}{T}\right] \tag{16}$$

For Eq. (16), $\ln\phi_p + 1 - \phi_p \approx -\phi_d^2/2$, $\phi_i \approx n_i v_i/(n_d v_d + n_p v_p)$ (i=d, p) and $v_p = N$ are used:

$$\mu_d = \left(\frac{\partial \Delta G}{\partial n_d}\right)_{\text{pr},T,n_p} = \text{const} + \ln\phi_d + \delta + \frac{b}{v_d}\rho\left[\phi_d - \ln\left(1-\phi_d\right)\right] - \phi_d - 2\phi_d \frac{b}{v_d}\frac{\Theta}{T} + \phi_d^2 \frac{b}{v_d}\frac{\Theta}{T} \tag{17}$$

where $const \approx v_d\chi + 1$.

Method of Calculation of *b*-Parameter for Nanoparticles that Can Point

Parameter *b* is defined as half of the restricted (excluded) volume between NPs and turns out to be half of the volume occupied by one NP when rotating in all directions:

$$b = \frac{\pi AL}{2} \tag{18}$$

where *A* is the surface area to rotate and *L* is the rotating length.

Method of Calculation of *b*-Parameter for a Rod Nanoparticle that Can Point

For a *rod* (*cf.* Fig. 1), *b*-parameter results:

$$b = \frac{\pi AL}{2} = \frac{\pi ld(l/2)}{2} = \frac{\pi l^2 d}{4} \tag{19}$$

where $A = ld$ and $L = l/2$.

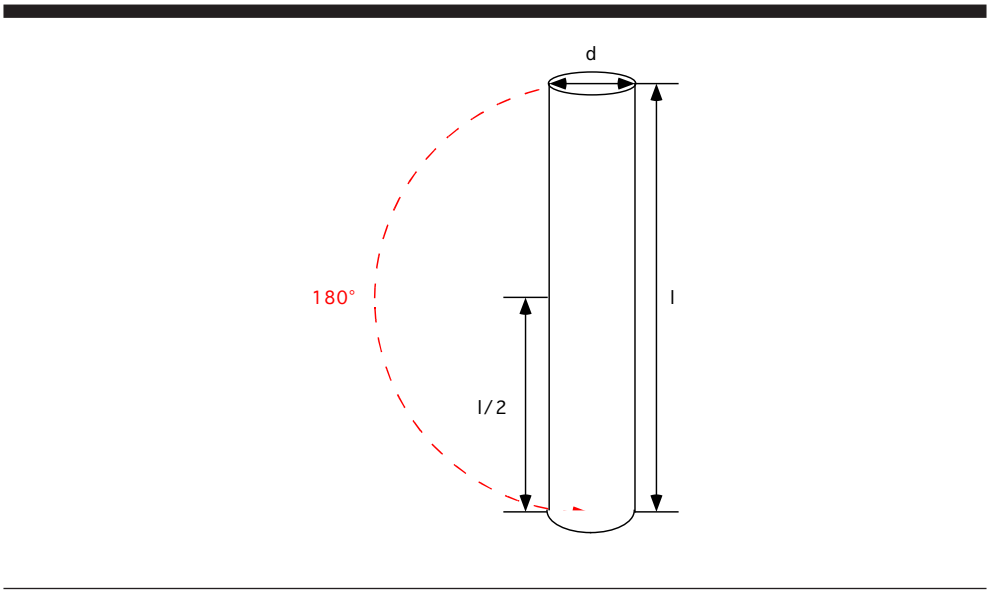

Fig. 1. Calculation of *b*-parameter for a rod.

Method of Calculation of *b*-Parameter for a Disc (Circular Sheet) NP that Can Point

For a *disc* (circular sheet, *cf.* Fig. 2), *b*-parameter results:

$$b = \frac{\pi AL}{2} = \frac{\pi\left(\pi D^2/4\right)(D/2)}{2} = \frac{\pi^2 D^3}{16} \tag{20}$$

where $A = \pi D^2/4$ and $L = D/2$.

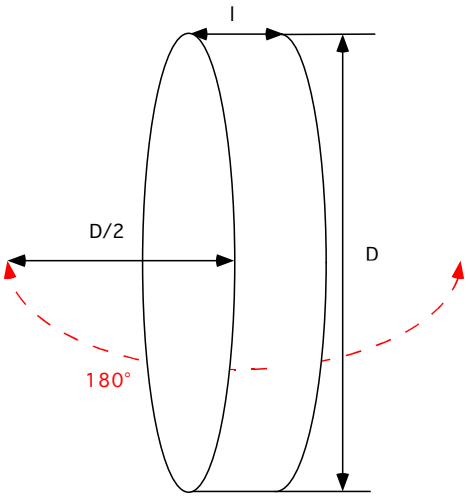

Fig. 2. Calculation of *b*-parameter for a disc (circular sheet).

Method of Calculation of *b*-Parameter for a Parallelepipedic-Sheet NP that Can Point

For a *parallelepipedic sheet* (*cf.* Fig. 3), *b*-parameter turns out to be:

$$b = \frac{\pi AL}{2} = \frac{\pi ah(h/2)}{2} = \frac{\pi ah^2}{4} \tag{21}$$

where $A = ah$ and $L = h/2$.

A *square sheet* is a particular case of parallelepipedic sheet with $h = a$ and its *b*-parameter results:

$$b = \frac{\pi AL}{2} = \frac{\pi h^2(h/2)}{2} = \frac{\pi h^3}{4} \tag{22}$$

where $A = h^2$ and $L = h/2$.

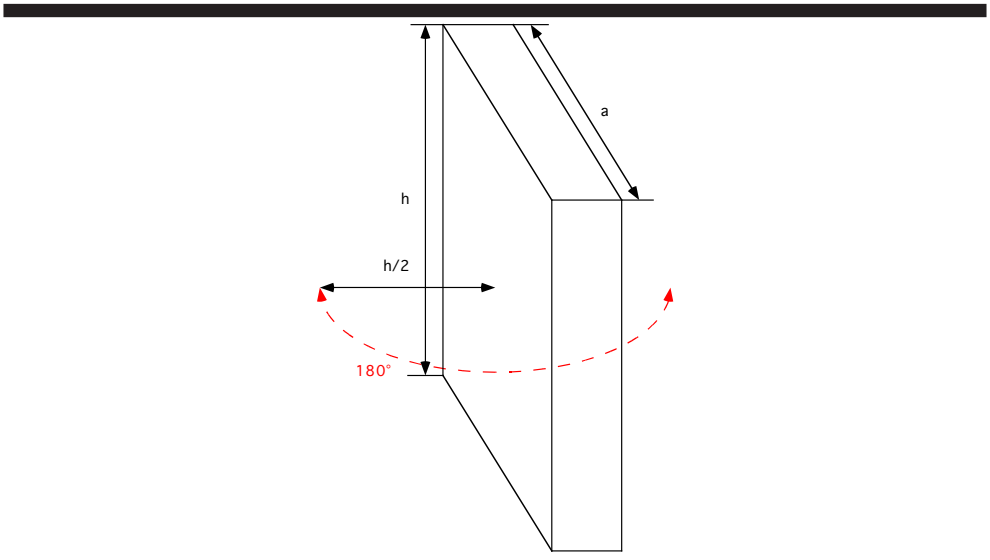

Fig. 3. Calculation of *b*-parameter for a parallelepipedic sheet.

Method of Calculation of *b*-Parameter for an Equilateral-Triangular-Sheet NP that Can Point

For an *equilateral-triangular sheet* (*cf.* Fig. 4), *b*-parameter results:

$$b = \frac{\pi AL}{2} = \frac{\pi\left(l^2/2\right)\sin(\pi/3)(2l/3)\sin(\pi/3)}{2} = \frac{\pi l^3 \sin^2(\pi/3)}{6} = \frac{\pi l^3}{8} \tag{23}$$

where $h = l\sin(\pi/3)$, $A = lh/2 = (l^2/2)\sin(\pi/3)$, $L = d = 2h/3 = (2l/3)\sin(\pi/3)$ and $\sin^2(\pi/3) = 3/4$.

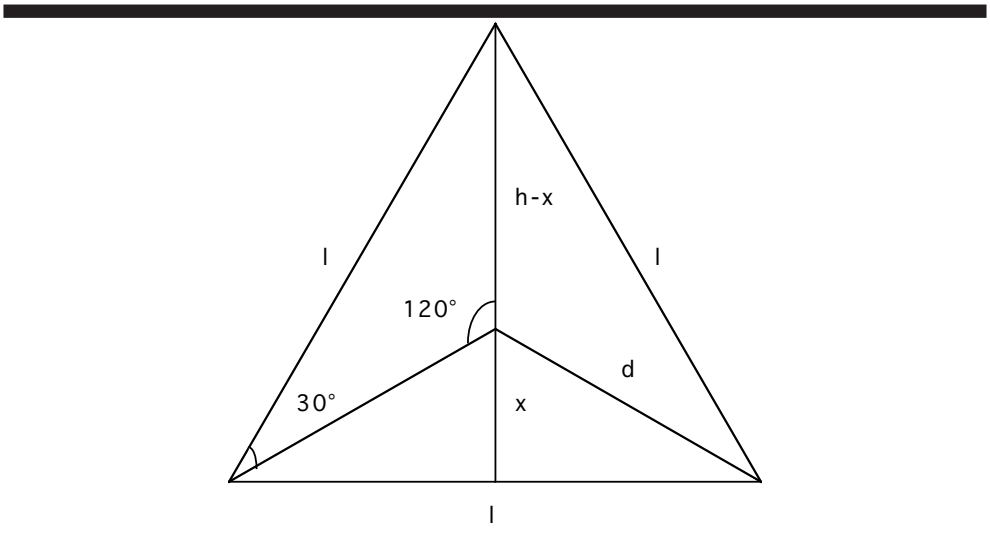

Fig. 4. Calculation of *b*-parameter for an equilateral-triangular sheet.

Method of Calculation of *b*-Parameter for a Regular-Hexagonal-Sheet NP that Can Point

For a *regular-hexagonal sheet* (*cf*. Fig. 5), *b*-parameter results:

$$b = \frac{\pi AL}{2} = \frac{\pi 3d^2 \cos(\pi/6) d \cos(\pi/6)}{2} = \frac{3\pi d^3 \cos^2(\pi/6)}{2} = \frac{9\pi d^3}{8} \tag{24}$$

where $a = 2d\cos(\pi/6)$, $A = 6d(a/2)/2 = 3da/2 = 3d^2\cos(\pi/6)$, $L = a/2 = d\cos(\pi/6)$ and $\cos^2(\pi/6) = 3/4$.

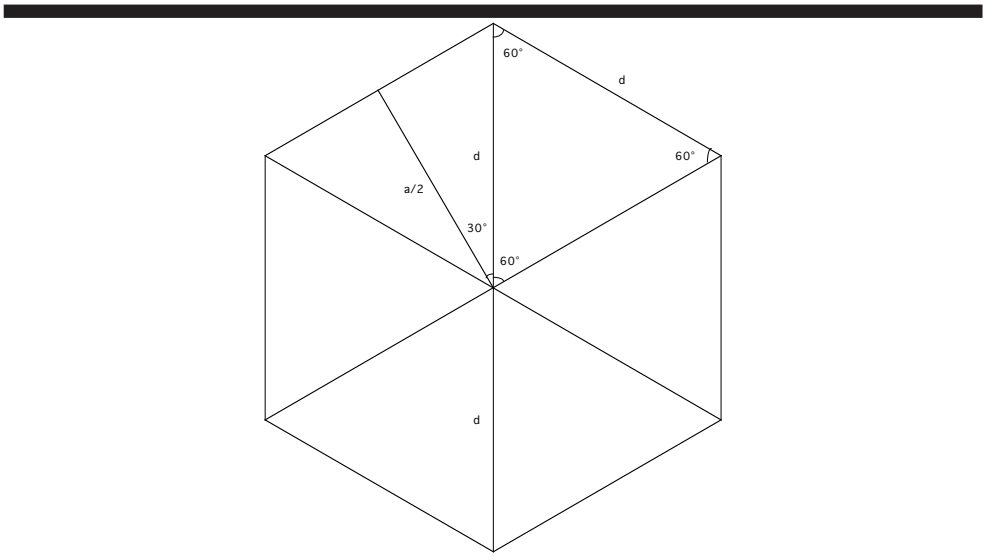

Fig. 5. Calculation of *b*-parameter for a regular-hexagonal sheet.

Method of Calculation of Phase Diagrams

In order to obtain PDs, one solves Eqs. (16) and (17) in view of (14) and (15), *i.e.*:

$$\phi_d^i + \frac{\left(\phi_d^i\right)^2}{1-\phi_d^i}\frac{b}{v_d}\rho^i - \left(\phi_d^i\right)^2 \frac{b}{v_d}\frac{\Theta}{T} = \phi_d^n + \frac{\left(\phi_d^n\right)^2}{1-\phi_d^n}\frac{b}{v_d}\rho^n - \left(\phi_d^n\right)^2 \frac{b}{v_d}\frac{\Theta}{T} \tag{25}$$

$$\begin{aligned} &\ln\phi_d^i + \delta^i + \frac{b}{v_d}\rho^i\left[\phi_d^i - \ln\left(1-\phi_d^i\right)\right] - \phi_d^i - 2\phi_d^i\frac{b}{v_d}\frac{\Theta}{T} = \ln\phi_d^n \\ &+ \delta^n + \frac{b}{v_d}\rho^n\left[\phi_d^n - \ln\left(1-\phi_d^n\right)\right] - \phi_d^n - 2\phi_d^n\frac{b}{v_d}\frac{\Theta}{T} \end{aligned} \tag{26}$$

For N, v_d and b, Θ/T rises with χ [Eq. (10)] so, in Eqs. (25) and (26), χ is identical in both phases and chemical potentials, assuming that χ does not vary with concentration, which permits solving algebraic mean-field equations [18–22]. Solving Eqs. (25) and (26), $\delta^i = 0$, $\rho^i = 1$, $\delta^n = 2\ln[-2/\pi^{1/2}(b/v_d)\ln(1-\phi_d^n)] - 1$ and $\rho^n = -2(v_d/b)/[\ln(1-\phi_d)]$ are supposed. From $\phi_d^i + \phi_p^i = 1$ and $\phi_d^n + \phi_p^n = 1$, ϕ_d^i, ϕ_d^n and Θ/T are unidentified. If values are given to Θ/T, ϕ_d^i and ϕ_d^n are calculated *via* Eqs. (25) and (26), and Θ/T *vs.* ϕ_d was shown, locating IP and NeP boundaries *via* cloud points ϕ_d^i and ϕ_d^n.

Computational Experiment

Systems of equations of PDs were numerically solved with code *Mathematica* (Wolfram Research, Inc., Champagne, IL), running on personal computers (PCs) with SuSE 10.0/CentOS Linux operating systems (OSs). Procedures were written in Mathematica *via* functions FindRoot[] (find roots) and Random[] (initial-guess chance location). In all cases, 1500 accidental initial-guess points were generated with the same solution being repeated in more than 90% of cases. In order to prove results self-consistency, five groups out of them were verified on an Apple Macintosh G5 PC (Tiger 10.4.10 OS).

Characterization of Modified Clay

X-ray Diffraction

Wide-angle X-ray diffraction (XRD) analysis characterized change in the gallery distance from unmodified to organically modified layered silicate clays. Patterns of XRD were obtained *via* a Rigaku Rotaflex powder diffractometer. An acceleration voltage of 50kV and current of 20mA were applied *via* Cu Kα radiation (λ = 1.5404Å). The layer spacing *d* of the compounds was calculated from measured *first-order reflection* (*n* = 1) reflection angles θ *via* Bragg equation:

$$n\lambda = 2d\sin(\theta) \tag{27}$$

The organoclay powder and the epoxy/organoclay hybrids were mounted on a sample holder with a large cavity, and a smooth surface was obtained by pressing it with a glass plate. Samples were scanned at diffraction angles (2θ) in 1–10° with a step scan of 0.02° per point and a scan rate of 0.5° per min. When mixed with prepolymer, organoclay <001> reflection shifted to lower angles θ would indicate the ability of the prepolymer to intercalate into the organoclay galleries.

Thermogravimetric Analysis

The thermogravimetric analysis (TGA) curves were measured in a Setaram Setsys 92-12 thermobalance under Ar flow. The temperature range was 25–1000°C with a heating rate of 10°C·min^{-1}.

Transmission Electron Microscopy

The morphological features were studied on a JEOL JEM-1010 transmission electron microscope (TEM) operated at an accelerated voltage of 100kV. The specimens for TEM were prepared in a Reichert–Jung Ultracut Microtome at RT.

Scanning electron microscopy

Scanning electron microscopy (SEM) images were taken on a Hitachi S-4100 (acceleration voltage of 20kV and working distances of 8–10mm) to analyze the fracture surface of the neat polymer and composites.

Stability of Epoxy/Montmorillonite Dispersions: Derjaguin–Landau–Verwey–Overbeek Theory

The variations of milieu ionic strength or p*H* modify the electrostatic forces, which grants control over the co-agulation processes. Derjaguin–Landau–Verwey–Overbeek [23,24] developed the research, which gives the total potential V_T as:

$$V_T = V_A + V_R \tag{28}$$

where V_T is total potential between two particles as the addition of attraction V_A and repulsion V_R potentials (*cf*. Fig. 6). Curve that represents total energy of interaction between colloidal particles (V_T) is adding of attraction (V_A) and repulsion (V_R) curves. It corresponds to an exponential equation, because the repulsion force is inversely proportional to the square of the distance, and the attraction force is also a function of the inverse of distance but this raised to an exponent greater than two.

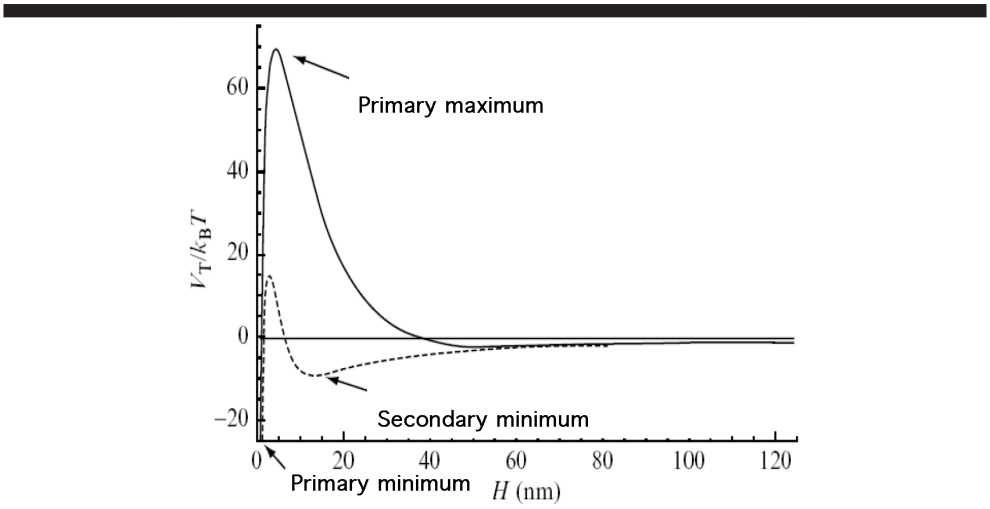

Fig. 6. Interaction potential *vs*. distance between the particles.

Rheological Oscillatory Measurements: Controlled-Stress Rheometer

Rheological oscillatory measurements were carried out in a controlled-stress rheometer (TA Instruments AR1000N), equipped with a parallel-plate geometry *via* 25mm-diameter plates at different temperatures. Samples thickness was 1mm. Dynamic rheology, performed under oscillatory test, is the preferred technique for detecting microstructural features. Stress sweeps at 10rad·s^{-1} were done to evaluate dispersions in viscoelastic behaviour at different temperatures (5, 25, 75, 120°C) and Nanofil concentrations. In order to evaluate viscoelastic-material characteristics, the frequency spectrum was examined showing the storage *G'* and loss *G"* shear moduli *vs*. frequency ω, which sweeps were executed at an oscillatory stress of 0.5Pa in the linear viscoelastic response (LVR) in 0.1–100rad·s^{-1} at 25°C. In order to study microstructural changes *vs*. temperature, heating and cooling temperature ramps were applied in 25–120°C at a frequency of 10rad·s^{-1} in LVR. Before every dynamic experiment, a steady pre-shear was achieved at a shear rate of 500s^{-1} for 5 min followed by a 120 min resting time. The procedure was necessary to erase any previous shear history and ensure that the material reached its equilibrium structure, so that the dispersions relaxed and were in the same reference state before mechanical solicitation. The effect of temperature on the rheological properties of dispersions is to produce a transition from a liquid-like behaviour (*G"* > *G'* at low temperatures) to a solid-like behaviour (*G'* > *G"* at temperatures above the transition).

CALCULATION RESULTS AND DISCUSSION

Solutions (*cf*. Figs. 7 and 8) are illustrated for monomer/disc systems (N = 1, D = 1).

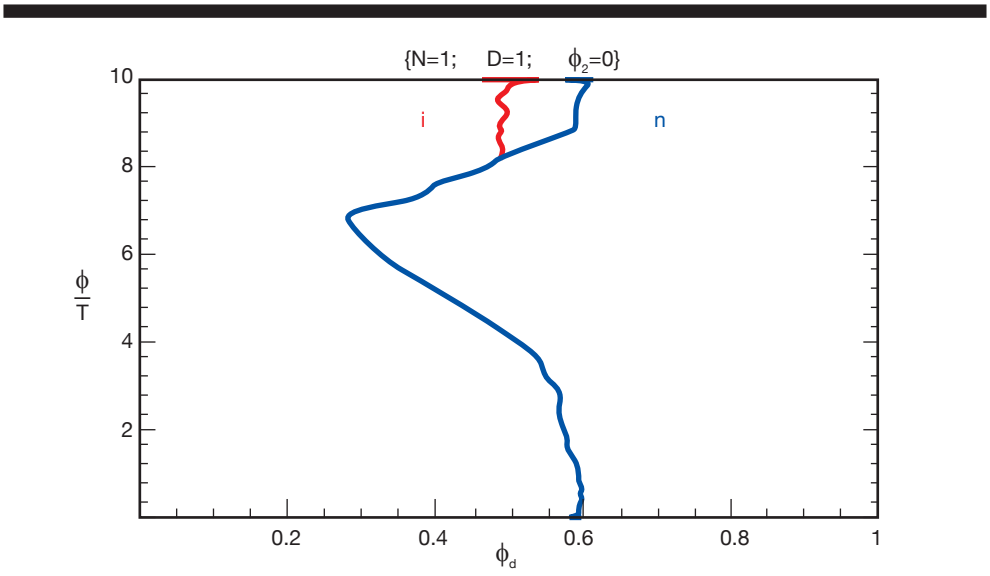

Fig. 7. Disc/polymer systems PD. Discs are mixed with monomer $N = 1$. Discs diameter $D = 1$. Plot Θ/T *vs.* ϕ_d. Area between phase boundaries encompasses immiscibility region. Miscible zones lie behind boundaries. In miscibility regions, *i* marks IP (*red*), and *n*, NeP (*blue*).

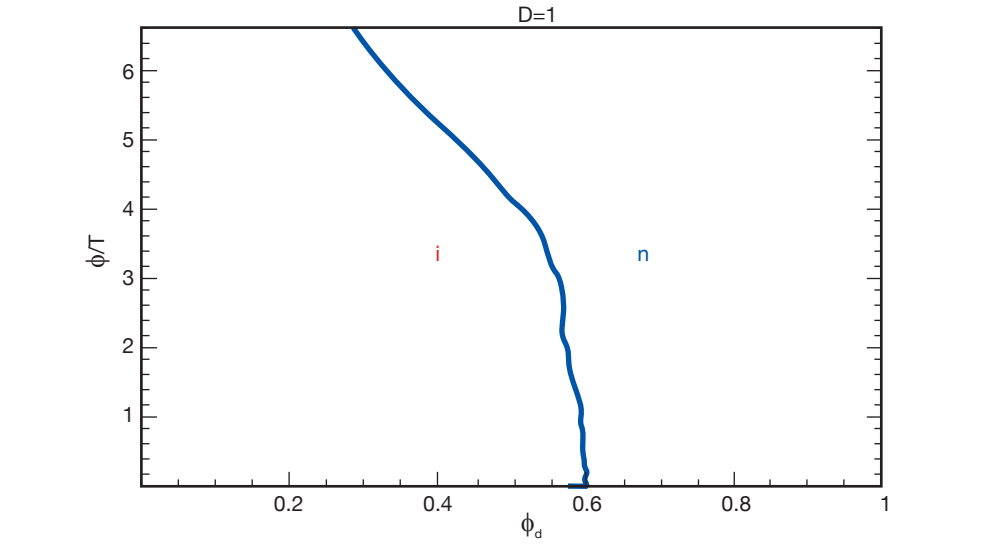

Fig. 8. Disc/polymer systems PD (detail). Notation is the same as in Fig. 7.

A comparison between nanodiscs, rigid molecules used for clay N757 organophilization and organophilic nanoclay N919 NCs follows. Nanoclay's homogeneous dispersion in the matrix at the nanometric level is significant to rise inorganic content and produce better molecular interactions. In order to attain a good dispersion, it is important to render layered silicates organophilic *via* ion exchange with alkylammonium cations, in order to achieve separation and

dispersion of the silicate layers within the epoxy matrix. Organophilization of N757 surface *via* ion exchange with cation surfactants produced the organosilicate with improved clay nanodispersions. Addition of cationic surfactant alkylic chains, *e.g.*, hydrophobic long-chain alkylammonium cations, *etc*. to N757 created nanolayers, bilayers, paraffin- and double-paraffin-type structures (*cf*. Fig. 9) [25]. A monolayer orientaton hinders epoxy-monomer intercalation between the organosilicate sheets [26]. Why did some intercalating agents make nanolayers, some others, bilayers and others, paraffin or double-paraffin arrays [27]? It depended on many factors, *e.g.*, molecule, stiffness, rotatable bonds, *etc*. However, a critical spacing of 4nm is not exceeded, because longer chains prefer to fold or are tilted to the basal plane of the clay mineral. Besides paraffin-type, *etc*. structures of the chains in all-*trans*-conformation, chain aggregates containing *gauche*-conformations were commonly formed [28]. The structures above are ideal. In N919, intersheet separation was 19.15Å, sheet length ranged 100–150nm, aspect ratio 50–80 and counter ions (*e.g.*, Na^+, K^+, Ca^{2+}) were exchangeable [29]. Dispersion of epoxy resins, *e.g.*, BPA, with N919 revealed that nanoclay is epoxy-intercalated, forming stable nanodispersions [30]. The exfoliation mechanism of the silicate platelets in epoxy resins follows: The driving force for the initial resin intercalation or diffusion into the clay galleries is the high surface energy of the clay, which attracts the polar resin molecule [31]. From the thermodynamic viewpoint, an N919 formed three types of lamellar NCs in rising order of overlap: flocculated < intercalated < exfoliated (individually dispersed) [32]. The sequence is also the succession of enhancement in properties [33]. Interlayer clay distance rises upon mixing with epoxy resin, leading to an intercalated and agglomerated organoclay sheets structure [34]. Resin curing time decayed with N919 because of cations' catalytic effect.

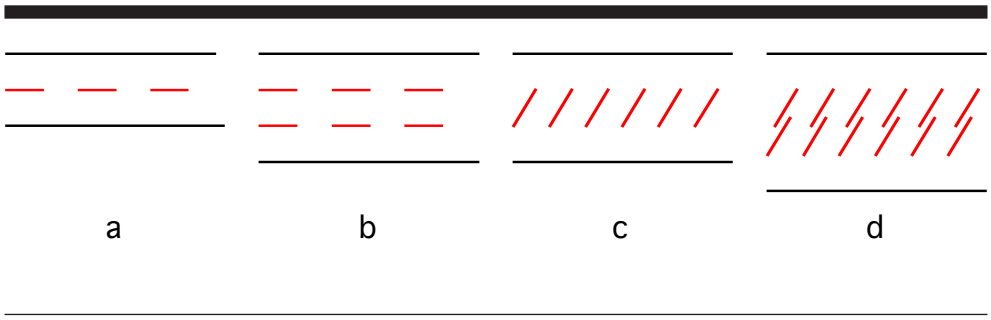

Fig. 9. Structures of alkylammonium cations between sheets:
a) monolayer; b) bilayer; c) paraffin-; d) double-paraffin-type.

CONCLUSION

From the previous computational method, calculation results and discussion, the following conclusions can be drawn.

1. Phase-diagram expressions were deduced in polymer/disc systems, analysing disc-size and temperature effects. Prediction of monomers/discs interactions gave criteria to advance mixing properties. The analysis used here is a good starting point for nanoindentation studies. Free-volume measurements showed complex behaviour (with some indication of a greater free volume in the systems where the clay is best dispersed), consistent with the lower glass transitions because of the reduced cross-link density of interfacial regimes.
2. This study extends the calculation of the restricted volume of disc nanoparticles to nanostructures with different shapes (rod, parallelepipedic sheet, equilateral-triangle sheet, regular-hexagonal sheet), in order to calculate nanocomposites' phase diagrams. The excluded volume was revealed as a powerful tool for investigating internal composites' nanostructures, *e.g.*, the dispersion state of the clay and the confinement effect of the silicate layers on the motion of the polymer chains. It was related to nanodispersions distortion or deformation, which resulted connected to the nanostructure present in the system.
3. Nanoclay homogeneous dispersion in the matrix increases inorganic content and improves molecular interactions. In order to attain a good dispersion, it is important to render layered silicates organophilic *via* ion exchange

with alkylammonium cations, in order to achieve separation and dispersion of the silicate layers in the matrix. The addition of these cations to sodium montmorillonite shows that a monolayer orientation hinders epoxy-monomer intercalation between the organosilicate sheets. The structures are ideal and further aggregation models are desired.

4. Interlayer clay distance rises upon mixing with epoxy resin, leading to an intercalated and agglomerated organoclay sheets structure. The nanocomposites show good compatibility and improvements in physical, mechanical, thermal and gas-barrier properties, electrical conductivity, decay in permeability and flammability, and rise in biodegradability. High-performance resins yield improved toughness and stiffness at the same time, despite the fact that improvement in both is difficult to achieve. Future research will deal with incorporating a more accurate description of polymer-mediated clay–clay interaction into the model, and obtaining direct phase-behaviour dependence on mixing chemical and molecular features. It will be interesting to see the possible generality of the present conclusions to the improved interaction models.

ACKNOWLEDGEMENT

The author wants to dedicate this manuscript to Prof. Dr. Agustín Campos, who was greatly interested in this research and would have loved to see its conclusion. He acknowledges financial support from Universidad Católica de Valencia *San Vicente Mártir* (Project Nos. PRUCV/2015/617 and 2017).

LITERATURE CITED

[1] F. Torrens, G. Castellano, Experimental studies for modelling the phase behaviour of monomer/polymer/disc composites, *Macromol. Symp*. **296** (2010) 557-565.
[2] F. Torrens, C. M. Gómez, L. M. León, C. Abad, A. Campos, Modelling studies of the phase behaviour of monomer/polymer/disk composites, *Macromol. Theory Simul*. **17** (2008) 325-340.
[3] F. Torrens, C. M. Gómez, I. S. Monzó, C. Abad, A. Campos, Modelling monomer/disc composites phase behaviour, *Macromol. Symp*. **311** (2012) 49-56.
[4] O. Becker, Y.-B. Cheng, R. J. Varley, G. P. Simon, Layered silicate nanocomposites based on various high-functionality epoxy resins: The influence of cure temperature on morphology, mechanical properties, and free volume, *Macromolecules* **36** (2003) 1616-1625.
[5] F. Torrens, G. Castellano, A. Campos, C. Abad, Negatively cooperative binding of melittin to neutral phospholipid vesicles, *J. Mol. Struct*. **834-836** (2007) 216-228.
[6] F. Torrens-Zaragozá, Polymer bisphenol-A, the incorporation of silica nanospheres into epoxy–amine materials and polymer nanocomposites, *Nereis* (3) (2011) 17-23.
[7] Y. Lyatskaya, A. C. Balazs, Modeling the phase behavior of polymer–clay composites, *Macromolecules* **31** (1998) 6676-6680.
[8] P. J. Flory, A. Abe, Statistical thermodynamics of mixtures of rodlike particles. 1. Theory for polydisperse systems, *Macromolecules* **11** (1978) 1119-1122.
[9] A. Abe, M. Ballauff, in: *Liquid Crystallinity in Polymers*, A. Ciferri, Ed., VCH, Weinheim (Ger.), 1991, pp. 131-131.
[10] A. Matsuyama, T. Kato, Theory of binary mixtures of a flexible polymer and a liquid crystal, *J. Chem. Phys*. **105** (1996) 1654-1660.
[11] L. Onsager. The effects of shape on the interaction of colloidal particles, *Ann. N. Y. Acad. Sci*. **51** (1949) 627-659.
[12] A. R. Khokhlov, A. R. Semenov, On the theory of liquid-crystalline ordering of polymer chains with limited flexibility, *J. Stat. Phys*. **38** (1985) 161-182.
[13] A. R. Khokhlov, A. R. Semenov, Theory of nematic ordering in the melts of macromolecules with different flexibility mechanisms, *Macromolecules* **19** (1986) 373-378.

[14] A. R. Khokhlov, in: *Liquid Crystallinity in Polymers*, A. Ciferri, Ed., VCH, Weinheim (Ger.) 1991, pp. 97-97.
[15] S. Pronk, D. Frenkel, Melting of polydisperse hard disks, *Phys. Rev. E* **69** (2004) 66123–1-7.
[16] T. Odijk, Theory of lyotropic polymer liquid crystals, *Macromolecules* **19** (1986) 2313-2329.
[17] P. J. Flory, *Principles of Polymer Chemistry*, Cornell University, Ithaca (NY), 1953.
[18] C. M. Gómez, I. Porcar, I. S. Monzó, C. Abad, A. Campos, Modelling the influence of nanoparticles in the phase behaviour of an epoxy/polystyrene mixture, *Eur. Polym. J*. **43** (2007) 360-373.
[19] J. E. Figueruelo, C. M. Gómez, I. S. Monzó, C. Abad, A. Campos, Modelling the influence of nanoparticles in the phase behaviour of an epoxy/polystyrene mixture, 2: Size and concentration dependences, *Macromol. Theory Simul*. **16** (2007) 458-475.
[20] C. M. Gómez, E. Verdejo. J. E. Figueruelo, A. Campos, V. Soria, On the thermodynamic treatment of poly(vinylidene fluoride)/polystyrene blend under liquid–liquid phase separation conditions, *Polymer* **36** (1995) 1487-1498.
[21] A. Campos, C. M. Gómez, R. García, J. E. Figueruelo, V. Soria, Extension of the Flory–Huggins theory to study incompatible polymer blends in solution from phase separation data, *Polymer* **37** (1996) 3361-3372.
[22] C. M. Gómez, J. E. Figueruelo, A. Campos, Evaluation of thermodynamic parameters for blends of polyethersulfone and poly(methyl methacrylate) or polystyrene in dimethylformamide, *Polymer* **39** (1998) 4023-4032.
[23] B. Derjaguin, L. Landau, Theory of the stability of strongly charged lyophobic sols and of the adhesion of strongly charged particles in solution of electrolytes, *Acta Physicochim. U. R. S. S*. **14** (1941) 633-662.
[24] E. J. W. Verwey, J. T. G. Overbeek, *Theory of the Stability of Lyophobic Colloids: The Interaction of Sol Particles Having an Electric Double Layer*, Elsevier, New York (NY), 1948.
[25] G. Lagaly, Interaction of alkylamines with different types of layered compounds, *Solid State Ionics* **22** (1986) 43-51.
[26] I. Mondragón, L. Solar, I. B. Recalde, C. M. Gómez, Cure kinetics of a cobalt catalysed dicyanate ester monomer in air and argon atmospheres from DSC data, *Thermochim. Acta* **417** (2004) 19-26.
[27] I. Porcar, L. Solar, C. Abad, C. M. Gómez, A. Campos, Preferential solvation of poly(methyl methacrylate) and a bisphenol A diglycidyl ether by size-exclusion chromatography, *J. Chromatogr,. A* **1031** (2004) 117-123.
[28] G. Kortaberria, L. Solar, A. Jimeno, P. Arruti, C. Gómez, I. Mondragon, Curing of an epoxy resin modified with nanoclay monitored by dielectric spectroscopy and rheological measurements, *J. Appl. Polym. Sci*. **102** (2006) 5927-5933.
[29] A. Nohales, L. Solar, I. Porcar, C. I. Vallo, C. M. Gómez, Morphology, flexural, and thermal properties of sepiolite modified epoxy resins with different curing agents, *Eur. Polym. J*. **42** (2006) 3093-3101.
[30] I. Mondragón, L. Solar, A. Nohales, C. I. Vallo, C. M. Gómez, Properties and struture of cyanate ester/polysulfone/nanocomposites, *Polymer* **47** (2006) 3401-3409.
[31] L. Solar, R. Navarro, C. Gómez, H. Reinecke, Layer spacing of montmorillonites modified with rigid rods, *J. Nanosci. Nanotechnol*. **7** (2007) 4546-4551.
[32] F. Torrens, L. Solar, V. Puchol, J. Latorre, C. Abad, A. Campos, Incorporation of silica nanospherical particles into epoxy-amine cross-linked materials, *Polym. Polym. Compos*. **16** (2008) 139-152.
[33] L. Solar, A. Nohales, R. Muñoz-Espí, D. López, C. M. Gómez, Viscoelastic behavior of epoxy prepolymer/organophilic montmorillonite dispersions, *J. Polym. Sci., Part B: Polym. Phys*. **46** (2008) 1837-1844.
[34] L. Solar, R. Muñoz-Espí, C. M. Gómez, Synthesis and properties of amine-cured epoxy/organophilic layered silicate nanocomposites, *Compos. Interf*. **16** (2009) 157-173.